ELSEVIER

Polymer 43 (2002) 6169–6181

polymer

www.elsevier.com/locate/polymer

Mechanical properties of silica–(meth)acrylate hybrid coatings on polycarbonate substrate

Victor A. Soloukhin[a,*], Willem Posthumus[a,1], José C.M. Brokken-Zijp[b,c,2], Joachim Loos[a,b,3], Gijsbertus de With[a,4]

[a]*Laboratory of Solid State and Materials Chemistry, Eindhoven University of Technology, P.O. Box 513, 5600 MB Eindhoven, The Netherlands*
[b]*Laboratory of Polymer Technology, Eindhoven University of Technology, P.O. Box 513, 5600 MB Eindhoven, The Netherlands*
[c]*Dutch Polymer Institute, P.O. Box 902, 5600 AX Eindhoven, The Netherlands*

Received 21 February 2002; received in revised form 31 July 2002; accepted 7 August 2002

Abstract

The mechanical properties of hybrid cross-linked coatings consisting of polymer (meth)acrylate matrices with dispersed nano-sized silica inorganic particles were determined. The coatings were deposited on polycarbonate substrates. It was shown that reliable elastic modulus and hardness data can be obtained from load and depth sensing indentation for a broad range of filler content when an indentation rate above 2 nm/s is used. The influences of a variation in coating thickness, filler content and chemical composition on these properties were combined with ATR-FTIR, TGA and TEM morphological analyses of the coatings. These analyses showed that filler content and chemical composition influence the mechanical properties of the silica–(meth)acrylate hybrid coatings in a complex way. © 2002 Elsevier Science Ltd. All rights reserved.

Keywords: Silica–(meth)acrylate hybrid coatings; Nano-indentation; Mechanical properties

1. Introduction

In the past decade, scientists have paid attention to a new type of coatings: hybrid organic/inorganic coatings [1–13]. The morphology of these coatings on a mesoscopic scale consists of at least an inorganic and an organic phase [1–8,14–19]. These coatings combine the flexibility and easy processing of polymers with hardness of inorganic materials and have been successfully applied on glass [10,12,13], metal [4] and polymeric [7,9,11] substrates. In general, these hybrid coatings are transparent, show a good adhesion, and enhance the scratch and abrasion resistant of a polymeric substrate.

Generally, the mechanical properties of a coating are very important, whatever the application might be. Load and depth sensing indentation, commonly referred to as nano-indentation, has shown itself as a powerful tool to characterize several mechanical properties of coatings [10,13,20–24] and has been broadly used for inorganic coatings for about ten years already [21,22,25–27]. On the contrary, for polymeric [11,24,28–30] (in particular hybrid [10,13,31]) coatings this technique is limitedly applied. It will be shown in the paper that this technique can be used to accurately estimate the hardness and the elastic modulus of cross-linked coatings on the basis of load–displacement data, originally proposed by Loubet et al. [32] and Doerner and Nix [23] and later significantly developed by Oliver and Pharr [22].

In this paper, load and depth sensing indentations with a Berkovich indenter were performed in order to evaluate the mechanical properties of hybrid coatings. The effective elastic modulus and the hardness were determined on the basis of the load–displacement data [22]. The reliability of the chosen analytical method was checked using different rates and a number of repeats and loads. The influence of coating thickness, filler content and chemical composition on the mechanical properties of the hybrid coatings was also investigated.

* Corresponding author. Tel.: +31-40-2473053; fax: +31-40-2445619.
E-mail addresses: v.a.soloukhin@tue.nl (V.A. Soloukhin), w.posthumus@tue.nl (W. Posthumus), j.brokken@tue.nl (J.C.M. Brokken-Zijp), j.loos@tue.nl (J. Loos), g.de.with@tue.nl (G. de With).
[1] Tel.: +31-40-2474964; fax: +31-40-2445619.
[2] Tel.: +31-40-2473742; fax: +31-40-2436999.
[3] Tel.: +31-40-2473033; fax: +31-40-2436999.
[4] Tel.: +31-40-2474947; fax: +31-40-2445619.

PII: S0032-3861(02)00542-6

This technique was tested on cross-linked polymer (meth)acrylate matrices with dispersed silane grafted nano-sized silica inorganic particles. These silica–(meth)acrylate hybrid coatings deposited on PC substrates were transparent and had a good adhesion.

Morphological analyses of the coatings were performed by means of ATR-FTIR spectroscopy, thermo-gravimetrical analysis (TGA) and transmission electron microscopy (TEM) to obtain better understanding of the factors influencing the mechanical properties of these coatings.

2. Experimental

2.1. Coating preparation

The modified nano-sized silica particles (5–15 nm) were prepared by mixing 100 g of colloidal silica dispersion (Ludox AS-30, 30 wt% suspension in water, ammonium stabilized; Aldrich) with 75 g of ethanol and 30 g of MEMO (3-(trimethoxysilyl) propyl methacrylate, a silane-coupling agent; ABCR) and heating them to reflux during 4 h. The amount of MEMO added was equal to about 10 molecules per nm^2 of silica surface. During the first 30 min of the reaction 125 g of *n*-propanol was added to compensate for the increasing hydrophobicity of the particles. After the reaction solvent was removed by distillation until a strong increase of the viscosity was observed. The amount of grafted MEMO on the silica particles was about 2 molecules per nm^2. The rest of MEMO was present as MEMO-oligomers [33]. The silica is expected to be present as separate particles due to their extensive grafting. The prepared dispersion was mixed with different (meth)acrylic monomers and a photoinitiator (Darocure 1173, 2-hydroxy-2-methyl-1-phenyl-propan-1-one; Aldrich) to obtain the final coating mixtures. These mixtures were applied on polycarbonate substrates by means of a Doctor Blade applicator. After evaporation of the solvent the coatings were cured by exposure to UV-light under a nitrogen atmosphere. Solid coatings were already obtained with a UV-dose of less than 300 mJ/cm^2, but a dose of 1000–1100 mJ/cm^2 was used to ensure that the cure for all the coatings was maximal [33]. Commercially available rectangular polycarbonate plates (bisphenol A polycarbonate) of 100 cm^2 and 0.2 cm thick (G.E. Plastics, The Netherlands) were used as substrates. The substrates were used as received apart after removing the protective sheets.

Fifteen silica–(meth)acrylate hybrid coatings different in silica content and/or thickness, and one coating without filler were prepared (see Table 1, also for the abbreviations of the compounds used). The chemical structures of the used (meth)acrylic monomers, MEMO and bisphenol A polycarbonate are given in Fig. 1.

All coatings had a good transparency and showed a good adhesion to the polycarbonate substrates.

Table 1
Prepared coatings with their chemical compositions and thickness h_f

Coating	Chemical composition		h_f (μm)
	Silica (vol%)	Organic matrix[a]	
1	20	IBMA/HDDA = 1/3	68.9
2	20	IBMA/HDDA = 1/3	56.1
3	20	IBMA/HDDA = 1/3	54.0
4	20	IBMA/HDDA = 1/3	43.4
5	20	IBMA/HDDA = 1/3	26.6
6	10	IBMA/HDDA = 1/3	70.0
7	30	IBMA/HDDA = 1/3	70.0
8	10	TMPTA	40.8
9	10	TMPTA/HDDA = 1/1	43.4
10	10	HEMA	33.2
11	10	HEMA/HDDA = 1/1	35.7
12	40	TMPTA	28.1
13	40	TMPTA/HDDA = 1/1	26.8
14	40	HEMA	20.4
15	40	HEMA/HDDA = 1/1	26.8
16	0	Ebecryl 745	16.6

[a] IBMA: isobornyl methacrylate; HDDA: 1,6-hexanediol diacrylate; TMPTA: trimethylolpropane triacrylate; HEMA: 2-hydroxyethyl methacrylate; Ebecryl 745: a commercially available acrylic mixture (UCB chemicals, Belgium) was used as a material for a coating without filler.

2.2. Coating thickness measurement

The thickness of the coatings was measured by means of optical microscopy after every mechanical test through monitoring a cross-section of every sample. All coatings have a thickness h_f in a range of 15–70 μm (Table 1). A typical image obtained is shown in Fig. 2.

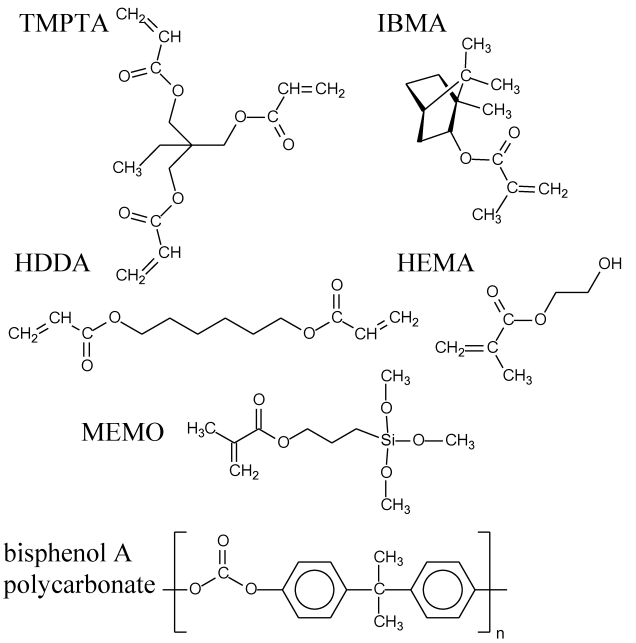

Fig. 1. Chemical structures of the used (meth)acrylic monomers, MEMO and bisphenol A polycarbonate.

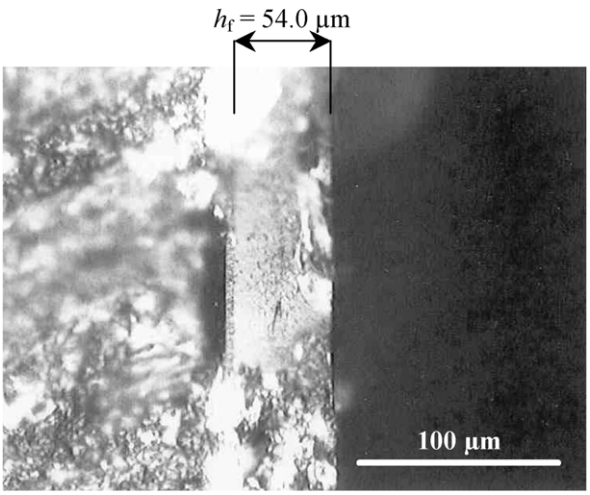

Fig. 2. An image of a coating–substrate cross-section by means of optical spectroscopy.

2.3. Load and depth sensing indentation

The elastic modulus and the hardness can be determined from indentation data obtained during one complete cycle of loading and unloading, shown in Fig. 3. The effective elastic modulus can be calculated using the following equation

$$E_{\text{eff}} = \frac{1}{\beta}\frac{\sqrt{\pi}}{2}\frac{S}{\sqrt{A}} \tag{1}$$

where A is the projected contact area, S is the experimentally measured unloading stiffness and β is a geometry constant, equal to 1.034 for a Berkovich indenter [34]. The projected contact area for a perfect Berkovich indenter is

$$A = 24.5h_c^2 \tag{2}$$

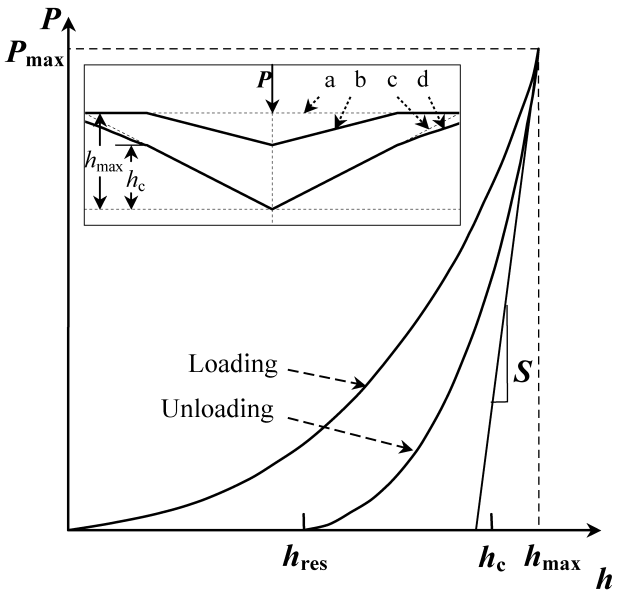

Fig. 3. A schematic representation of load P versus indenter displacement h. (a) Initial surface; (b) surface profile after load removal; (c) indenter; (d) surface profile under load [22].

where h_c is the contact displacement (or the contact depth). For a non-ideal indenter typically a polynomial in h_c is used. The contact depth, along which contact is made between the indenter and a specimen, can be estimated from the load–displacement data

$$h_c = h_{\max} - \epsilon\frac{P_{\max}}{S} \tag{3}$$

where $h_{\max}$ is the maximum displacement, which corresponds to $P_{\max}$, the maximum load, and ϵ is a constant, which depends on the geometry of the indenter, equal to 0.75 for a Berkovich indenter [22]. The unloading stiffness, which is the slope of the unloading curve during the initial stage of unloading, $S = \mathrm{d}P/\mathrm{d}h$, can be obtained by fitting the unloading curve by

$$P = B(h - h_{\text{res}})^m \tag{4}$$

and taking the derivative at the maximum displacement, $h = h_{\max}$. Here P is the indentation load, h is the displacement, B and m are fitting parameters and h_{res} is the residual displacement after complete unloading. The effective elastic modulus, used because elastic deformation occurs in both the specimen and the indenter, is related to the specimen elastic modulus by

$$\frac{1}{E_{\text{eff}}} = \frac{1-\nu^2}{E} + \frac{1-\nu_i^2}{E_i} \tag{5}$$

where E and ν are Young's modulus and Poisson's ratio for the specimen, respectively, and E_i and ν_i are the same quantities for the indenter. For the diamond $E_i = 1141$ GPa and $\nu_i = 0.07$ [35] were used.

Finally, the hardness H is defined from:

$$H = \frac{P_{\max}}{A} \tag{6}$$

In the case of a coating–substrate system, E and H represent apparent values, which combine mechanical properties of both the coating and the underlying substrate if a broad range of loads is used. The measurements can be represented as a couple of E_{app} and H_{app} curves, as schematically shown in Fig. 4, where gradual changes of the apparent elastic modulus E_{app} and the apparent hardness H_{app} correspond to the elastic modulus E_f and the hardness H_f of the coating for very shallow displacements, and to the

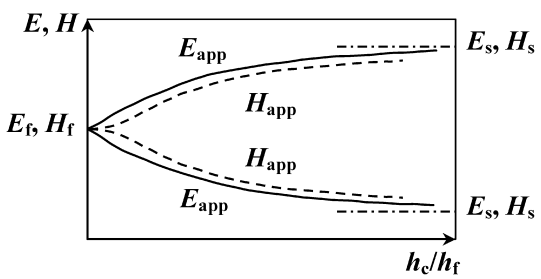

Fig. 4. A schematic representation of the apparent elastic modulus E_{app} and hardness H_{app} versus relative indenter displacement h_c/h_f [36].

elastic modulus E_s and the hardness H_s of the substrate for very deep displacements. Typical behaviors of E_{app} and H_{app} for two common situations ($E_f > E_s$ and $H_f > H_s$) and ($E_f < E_s$ and $H_f < H_s$) are shown in Fig. 4 [36].

For this paper indentation experiments were carried out at room temperature and ambient atmosphere using a home-built apparatus. The apparatus permitted up to 25 indentations to be made in one run at loads ranging from 2 to 1000 mN with a range of possible rates from 0.4 to 20 nm/s. A Berkovich-type diamond indenter was used. The apparatus only allowed experiments under displacement control to be performed. The calibration procedure suggested by Oliver and Pharr [22] was used to correct for the load frame compliance of the apparatus and the imperfect shape of the indenter tip. The area function of this indenter was calibrated using B270 glass (Schott, Jena, Germany), whose elastic modulus was determined independently as 75 ± 1 GPa using the pulse-echo method. The compliance of this system as determined from the unloading curve was 0.0003 μm/mN and the projected area of the indenter A was related to the contact depth h_c of the indentation by $A = ah_c^2 + bh_c$ ($a = 24.5$ and $b = 5.71$ μm), being equivalent to a tip radius of approximately 0.9 μm. The calibration was performed using B270 glass for a depth range of 0.1–2.9 μm, where the maximum indentation depth was restricted by the load limitation [10].

Phenomena such as pile-up and sink-in, which may lead to some overestimate or underestimate of the contact area and consequently to errors for the elastic moduli and the hardness [34,37], were not taken into account.

2.4. Morphology investigation

Attenuated total reflection infrared spectroscopy (ATR-IR) was used as the main tool for morphological analysis. Infrared spectra were recorded using ATR objective of a Biorad UMA 500 microscope coupled to a Biorad FTS 6000 FTIR spectrometer. The IR spectra were recorded with a resolution of 4 cm^{-1} adding 50 scans. A slide-on ATR crystal of germanium was used permitting investigating about 1 μm thick upper layers of the coatings. A typical area for collecting ATR-IR information of a coating was about 100×100 μm^2.

For investigating the chemical composition over the thickness of a coating, a 5 μm thick slice of coating 1 was made by means of microtome cutting. A schematic drawing of the slice is shown in Fig. 5. Five FTIR spectra from five different regions in the slice were obtained. The approximate locations of the five investigated regions ($\sim 25 \times 25$ μm^2 each) are shown in Fig. 5. From the slice IR spectra were recorded using the IR microscope in the transmission mode of an area of about 625 μm^2 selected by means of redundant aperturing.

TGA performed at a temperature range of 30–900 °C was used for checking silica content in each of the coatings

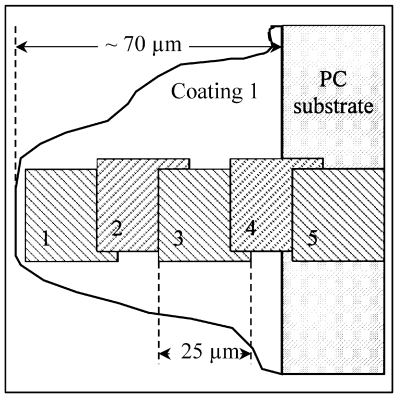

Fig. 5. A schematic draw of a 5 μm thick slice made of coating 1 for FTIR analysis.

at a decomposition temperature of 900 °C. The analysis was performed by means of Pyris 6 thermo-gravimetrical analyzer (Perkin Elmer). A powdered sample was obtained by means of scratching the coating from the substrate.

Additionally, TEM was used. Thin cross-sectional cuts of the coatings 8, 11 and 15 were prepared at room temperature using a Reichert-Jung Ultracut E microtom. For TEM investigations the cross-sections were transferred on conventional Cu grids. TEM-work was performed using a Jeol 2000FX operated at 80 kV in order to enhance the contrast between the polymer matrices and the silica particles.

Optical microscopy was also used for an observation of the coating morphology and for the visualization of the final indents. As an example we show the optical micrograph of 1 N load imprints after nano-indentation in three IBMA/HDDA coatings with different silica content (coatings 6, 1 and 7) in Fig. 6. As clearly can be seen from the size decline of the imprints in Fig. 6, the higher the silica content, the higher the hardness of the coatings. The indenter displacement versus load responses of these 70 μm thick coatings for the range of applied loads (4–1000 mN) are shown in Fig. 7. The responses unambiguously show that the higher the silica content, the smaller the indentation depth and consequently the smaller the contact area, in line with the sizes of the imprints in Fig. 6 (see also Section 3.3).

For evaluating the glass transition temperature T_g of the silica–(meth)acrylate hybrid coatings, a differential scanning calorimeter (DSC) Pyris 1 (Perkin Elmer) with temperatures ranging from −20 to +90 °C, and a heat rate of 10 and 50 °C/min was used. Similar to TGA a powdered sample was obtained by means of scratching the coating from the substrate. Unfortunately, no reliable T_g of the silica–(meth)acrylate hybrid coatings was obtained yet, although in the case of polycarbonate, the expected T_g, equal to 150 °C, was successfully found. This may be due to selective sampling by the scratching procedure and/or the presence of a broad T_g signal.

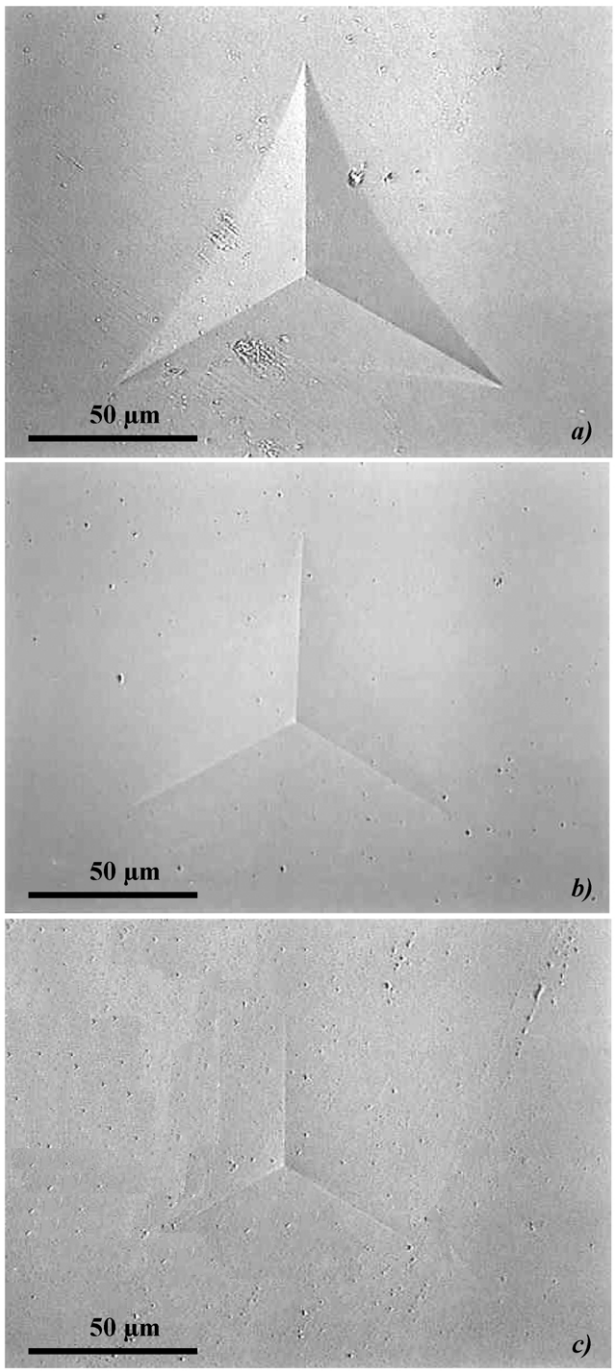

Fig. 6. Optical micrographs of the 70 µm thick silica–IBMA/HDDA hybrid coatings after nano-indentation tests with a load of 1 N. The coatings have different silica content 10 (a), 20 (b), and 30 vol% (c), respectively.

3. Results and discussion

3.1. Reliability of load and depth sensing indentation measurements

Although load and depth sensing indentation has been already thoroughly investigated in the case of thermoplastic polymers and hybrid coatings [10,13,31,38 see also 39 for the features of the technique itself], it has not been yet explicitly checked for cross-linked polymers. There is only one paper known to us, which partly dealt with this [40]. Thus, it makes sense to perform a set of experiments, which would expose possible errors during the measurements and/or their further interpretations. Among such experiments the dependence of the indentation rate and the influence of the number of repeats of indentations for a fixed rate at the same position are of primary interest.

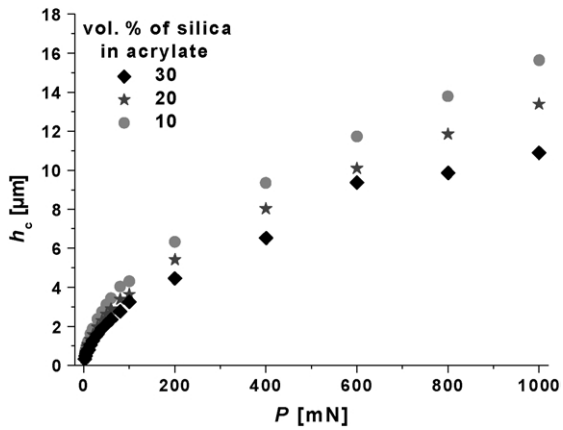

Fig. 7. The indenter displacement versus load for the 70 µm thick silica–IBMA/HDDA hybrid coatings with different silica content.

Rate-dependent indentations were performed on coating 1 (Table 1) with rates r ranging from 0.5 to 20 nm/s, with three repeats at the same position and an applied load of 10 mN. The experiments show that the contact displacement h_c on the average is equal for the rates from 2 to 20 nm/s and slightly lower for the rates 0.5 and 1.0 nm/s. The results for the effective elastic modulus and the hardness are represented in Fig. 8(a) and (b). Thus on the average and including possible inhomogeneity of the coating on 1–50 µm level, the obtained E_{eff} and H data are independent of rate, if $r \geq 2$ nm/s is used.

Repetitive indentation at the same position was done as follows. The indenter, once it reached the maximum load $P_{\max}$ is unloaded until 10% of $P_{\max}$, then the next indentation is set at the same position up to the same $P_{\max}$ with a maximum of 10 repeats. The indenter is totally unloaded after the last repeat. The value of E_{eff} and H was calculated for every unloading curve. Satisfactory reproducibility of E_{eff} and H values for all repeats shows that apart from the first loading during all the next ones no non-reversible plastic deformation occurred and the E_{eff} and H values obtained represent their correct values for the sample.

For the silica–(meth)acrylate hybrid coatings two sets of 'repeating' indentations at the same position were performed. Coating 1 was used for both sets. The first set consisted of five rates (0.5, 1, 5, 10 and 20 nm/s) and of five loads (2, 4, 10, 20 and 50 mN). Six repeats of indentations

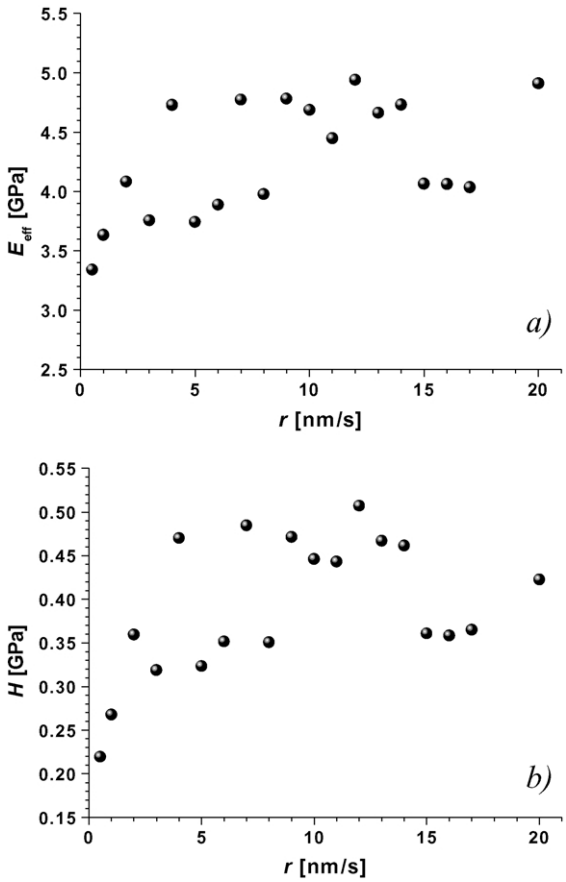

Fig. 8. The effective elastic modulus (a) and the hardness (b) versus rate corresponding to a load of 10 mN for coating 1.

were used for every combination of rate and load. The measurements show that for the low rates 0.5 and 1 nm/s h_c increases over all six repeats and consequently the values of E_{eff} and H change. Starting from a rate of 5 nm/s no further obvious changes in h_c, and consequently in E_{eff} and H, are observed. Varying the loads does not show any noticeable influence on the values of the mechanical properties among all repeats for the range of rates used. As can be noticed, the results of this set are in a good agreement with above discussed rate measurements, where a small rate dependence was observed for the low rates 0.5 and 1 nm/s as well. So relying on these two independent sets of measurements it can be concluded that at the above rate of 5 nm/s no rate and no repeating dependences on the mechanical properties of the silica–(meth)acrylate hybrid coatings should be expected. For all further experiments a rate of 10 nm/s was used.

For checking if any repeating dependence can be observed for the range of applied loads, a second set of measurements was carried out. The measurements were performed for three repeats in a row and with three different loads (100, 400 and 1000 mN) on coating 1. No obvious differences between E_{eff} and H were found.

Since all coatings are applied on polycarbonate substrates, it seems logical and necessary to estimate E and H of polycarbonate by means of nano-indentation as well, and to compare the obtained values with literature data. Such measurements were performed at the beginning of the experiments and repeated regularly over the period of the experiments in order to assess possible changes in substrate properties. The obtained data E of polycarbonate lie in the range of 2.10–2.47 GPa in good agreement with earlier published data for the elastic modulus of polycarbonate: 2.3 GPa after tensile testing [41] and using an integrated microindenter [42]. The elastic modulus of polycarbonate was recalculated from its effective values (2.50–2.94 GPa) using Eq. (5) and Poisson's ratio of polycarbonate, $\nu = 0.4$ [41].

The values for H obtained, in the range from 0.135 to 0.150 GPa, are deviating somewhat from the hardness of 0.17 GPa also obtained by nano-indentation [11].

The above-mentioned range of about 15% for E and H, besides the error of measurements (about 10%), may be also due to ageing of polycarbonate top layer [43].

3.2. Influence of coating thickness on the mechanical properties

To test the influence of coating thickness on the mechanical properties, a series of chemically identical coatings but with a different thickness was produced. The series consists of five hybrid coatings, which contain 20 vol% of silica in IBMA/HDDA (coatings 1–5 in Table 1) with a thickness of 68.9, 56.1, 54.0, 43.4 and 26.6 μm, respectively. The experimental data for the effective elastic modulus E_{eff} and the hardness H versus relative indenter displacement h_c/h_f for these five coating–substrate systems are shown in Fig. 9(a) and (b), respectively. The curves show the typical response of a coating–substrate system with $E_f > E_s$ and $H_f > H_s$ (Fig. 4). Deeper penetration of the indenter into a coating corresponds to a higher contribution of the underlying substrate to the measured values of the mechanical properties for a coating–substrate system. From the measured values a tendency for approaching E and H magnitudes for polycarbonate can be clearly observed. Remember that in our case the measured values of the effective elastic modulus for polycarbonate are in a range of 2.50–2.94 GPa.

The depicted curves do not show the expected plateaus at shallow indenter depth, which correspond to E_{eff} and H of the coatings without any influence of the substrate. Earlier reported plateaus occurred when relative indenter depth is less than 0.07 [13], and 0.40 [24]. An optical observation of the imprints suggested that in some cases slight sink-in occurred whereas in the others sink-in was combined with slight pile-up. It is believed that a rather complex combination between sink-in and pile-up at shallow indentation depths might be an explanation for the absence of the plateaus. The absence of the obvious plateaus in our experiments makes estimates of E_{eff} and H for the coatings

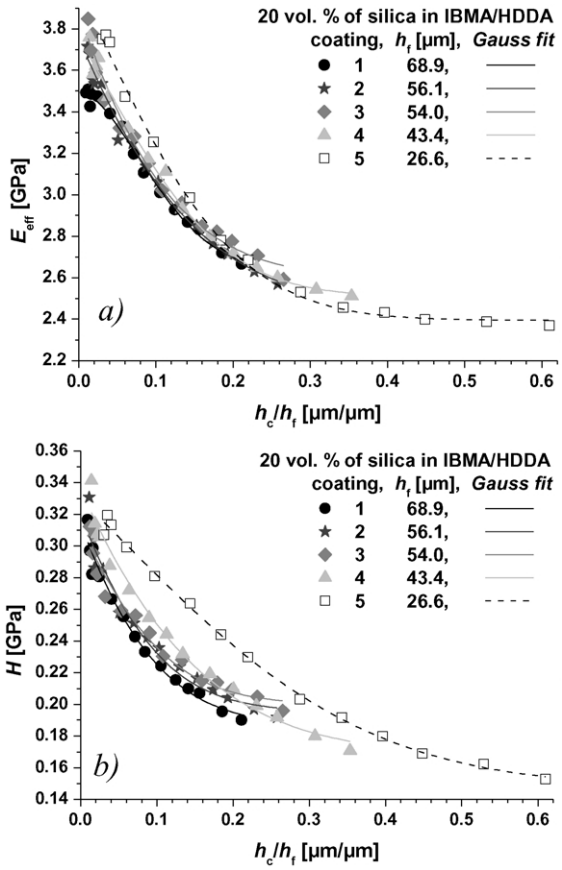

Fig. 9. The effective elastic modulus (a) and the hardness (b) versus relative indenter displacement for the silica–IBMA/HDDA hybrid coatings with 20 vol% of silica and a different thickness.

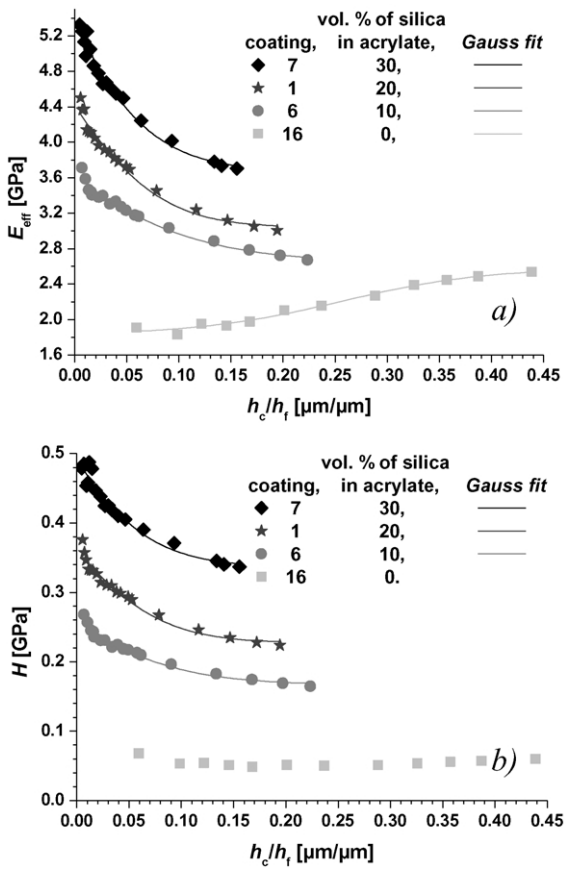

Fig. 10. The effective elastic modulus (a) and the hardness (b) versus relative indenter displacement for the 70 μm thick silica–IBMA/HDDA hybrid coatings with different silica content.

more difficult. Two functions were used to fit the data obtained with the Origin 6.0 software. It appeared that a Gaussian function

$$y = C_1 + \frac{C_2}{C_3\sqrt{\pi/2}}\exp\{-2\frac{(x-C_4)^2}{C_3^2}\}$$

where C_1, C_2, C_3 and C_4 are the fitting parameters, respectively, results in a slightly better fit to the date than a second order polynomial: $y = B_1 + B_2x + B_3x^2$, where B_1, B_2 and B_3 are the fitting parameters, respectively. Since the values obtained from extrapolation of the Gauss and polynomial fittings to the ordinate axis (E_{eff} and H for $h_c/h_f = 0$) generally agree within 2%, extrapolated values are insensitive to the function used. The values obtained from a Gauss extrapolation were taken as the final E_{eff} and H values for the coatings.

The good agreement of the various curves, especially in the case of $E_{eff} = f(h_c/h_f)$, shows the reliability of load and depth sensing indentation for the tested coatings with a different thickness. Since no thickness dependence on mechanical properties was found, the method can be applied on the silica–(meth)acrylate coatings.

3.3. Influence of the chemical composition on the mechanical properties

The influence of the chemical composition (CC) on the mechanical properties within the silica–(meth)acrylate hybrid systems is the main interest in the work. The first series consists of three silica–IBMA/HDDA hybrid coatings with a thickness of about 70 μm and a silica content of 10, 20 and 30 vol% (coatings 6, 1 and 7 in Table 1), respectively. Optical microscopy of the indentations show that the higher the silica content, the higher the hardness of the coatings (see Section 2.4) and therefore an increase in the elastic modulus in general is expected too. This is indeed the case when these coatings are compared with an acrylate coating without filler (Figs. 10 and 11). Similar to the thickness series, any evident plateau at low loads is absent for the silica-filled coatings (Fig. 10), although, for the coating without silica a plateau can be found for E_{eff} for $h_c/h_f < 0.15$ and for H for $h_c/h_f < 0.3$.

To assess whether silica content mainly defines the mechanical properties of the silica–(meth)acrylate hybrid coatings, a second series of the silica-filled hybrid coatings with varying organic matrices was made. The coatings with 10 and 40 vol% of silica particles were used. TMPTA and

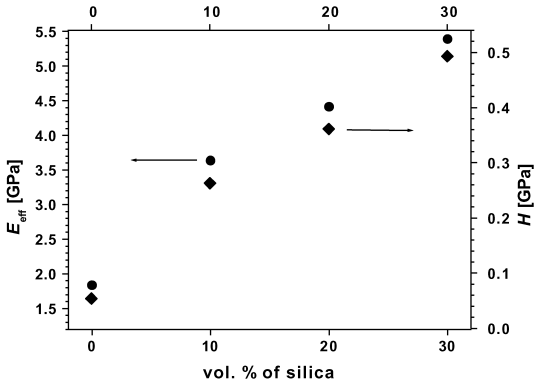

Fig. 11. The effective elastic modulus (black) and the hardness (gray) versus vol% of silica in the silica–(meth)acrylate hybrid coatings (coatings 16, 6, 1 and 7).

HEMA were chosen as new organic matrices. Additionally, HDDA was used as a cross-linking modifier in combination with TMPTA and HEMA. The addition of HDDA to TMPTA decreases, in principle, the cross-link density (XLD) by lowering the functionality of the starting monomer mixtures (Fig. 1). On the contrary, the addition of HDDA to HEMA enhances the functionality of the starting monomer mixtures and therefore increases, in principle, the cross-link density (Fig. 1). The effective elastic modulus and the hardness for each coating within the series are given in Table 2.

The analysis of the data shows that a change of organic matrix has a significant effect on the effective elastic modulus and the hardness of the silica–(meth)acrylate hybrid coatings. In the case of TMPTA matrix an increase of silica content from 10 up to 40 vol% (coatings 8 and 12) does not increase the value of E_{eff} within the error of measurements, although the hardness increases approximately by 1.3. A decrease of XLD in the system, by means of adding HDDA, leads to an increase in E_{eff} by a factor of 3.4 and in H by 4.2 when the silica content is increased from 10 up to 40 vol% (coatings 9 and 13). In the case of HEMA and HEMA/HDDA matrices an increase in E_{eff} by 1.2 and in H by 2.6 (coatings 10 and 14), and by 3.7 and 6.3 (coatings 11 and 15) occurs for the same increase in silica content, respectively.

Table 2
The effective elastic modulus E_{eff} and the hardness H of coatings 8–15

Coating	Chemical composition		E_{eff} (GPa)	H (GPa)
	Silica (vol%)	Organic matrix[a]		
8	10	TMPTA	7.61	0.668
9	10	TMPTA/HDDA = 1/1	3.38	0.261
10	10	HEMA	6.34	0.262
11	10	HEMA/HDDA = 1/1	1.88	0.103
12	40	TMPTA	7.59	0.860
13	40	TMPTA/HDDA = 1/1	11.48	1.092
14	40	HEMA	7.73	0.657
15	40	HEMA/HDDA = 1/1	6.99	0.651

[a] See Table 1.

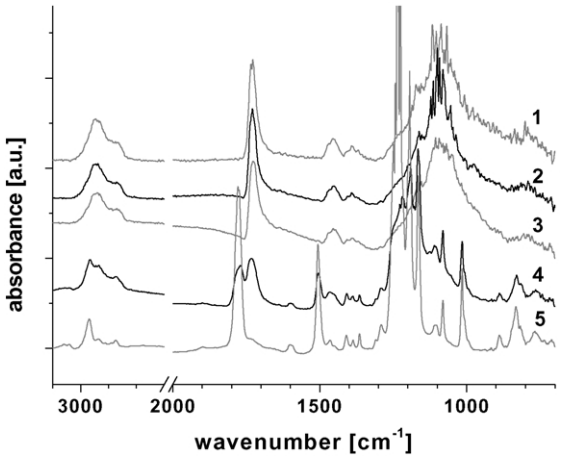

Fig. 12. Corresponding transmission FTIR spectra taken from five different regions of a 5 μm thick slice, which is made of coating 1.

A comparison between coatings 8 and 9 with 10 vol% of silica shows that a decrease in XLD which corresponds to a decrease in E_{eff} and H by a factor of 2.3 and 2.6, respectively. A contradicting phenomenon can be found when HEMA is exchanged for HEMA/HDDA (coatings 10 and 11). Here a decrease by 3.4 and 2.5 for E_{eff} and H, respectively, takes place, whereas XLD increases.

A comparison between coatings 12 and 13 with 40 vol% of silica shows that a decrease in XLD corresponds to a slight increase in E_{eff} and H by a factor of 1.5 and 1.3, respectively. In the case of the HEMA and HEMA/HDDA coatings (coatings 14 and 15) insignificant changes in E_{eff} and H occurred, although XLD is larger in the latter one.

Additionally, it is worth mentioning that for all silica–(meth)acrylate hybrid coatings containing 10 vol% of silica, no surface cracks occur for the range of applied loads (4–1000 mN). As the silica content is increased up to 40 vol%, surface cracks occur on all coatings under high loads ($\geq$800 mN). Crack formation is accompanied with typical changes in load–displacement curves [10,12]. These curves were not taken into account in the data presented here.

Some deviations in E_{eff} and H for coating 1 between the rate series, the thickness series and the silica content series are probably due to an ageing effect. This will be discussed in detail elsewhere [43].

3.4. Morphological analysis of the coatings

Morphological analysis of the coatings can bring deeper insight into mechanical properties and the physical and chemical phenomena responsible. ATR-FTIR spectrometer was employed as the main tool for morphological analysis in the work.

Firstly, the homogeneity of the coatings was investigated. ATR-IR analysis showed that the chemical composition of the coatings is homogeneous over the surface in a

Table 3
Characteristic IR frequencies for silica–(meth)acrylate coatings on polycarbonate substrate

Assignment	Wavenumber (cm^{-1})
Antisymmetric CH_3 stretching	2969–2965
Antisymmetric CH_2 stretching	2929–2912
Symmetric CH_3 stretching	2884–2883
Symmetric CH_2 stretching	2861–2849
C=O stretching	*1782*
C=O stretching	1740–1715
C=C stretching	1690–1650
Aromatic ring stretching	*1600, 1515*
CH_3 symmetric bending	1473–1446
CH_2 scissor	1460–1445
CH_3 antisymmetric bending	1385–1368
C–O stretching	*1219, 1168, 1158*
Ring breathing	*1188, 1112, 832*
C–O stretching	1154
Si–O–Si stretching	1090, 1020, 820
Aromatic C–H out-of-plane deformation	*785–700*

Italics correspond to polycarbonate peaks.

thickness of 1 μm. The transmission IR spectra of coating 1 for regions from 1 to 5 (Fig. 5) are shown in Fig. 12. The spectra of the first three regions show satisfactory homogeneity within the coating throughout its thickness, as can be concluded from the negligible deviations between ratios of the peak areas for corresponding chemical bond deformations: the symmetric and antisymmetric C–H stretching of the CH_3 and CH_2, C=O stretching, symmetric and antisymmetric CH_3 bending, and the CH_2 'scissor' (Table 3 and see also Fig. 1) [44].

The spectrum taken from the region 4 represents the coating as well as the polycarbonate substrate, whereas the spectrum taken from the region 5 shows only the polycarbonate substrate itself. As can be seen, deformations of the aromatic rings in bisphenol A polycarbonate (Fig. 1) change the spectrum profile dramatically (spectrum 5 in Fig. 12): see the corresponding frequencies for aromatic ring stretching, ring 'breathing' and for aromatic C–H out-of-plane deformation. Additionally, new significant peaks at frequencies of 1782 and roughly 1230–1150 cm^{-1} for C=O and C–O stretching of the carbonate groups can be found, respectively. Spectrum 4 is indeed a combination of the spectra of the polycarbonate substrate and the silica–IBMA/HDDA coating. Hence, coating 1 is homogeneous within the fault of measurement.

The corresponding ATR-IR spectra taken for the coatings, which are only different in thickness, are represented in Fig. 13 (coatings 1–5 in Table 1). It appeared that, four of the five spectra are identical, indicating good similarity in chemical compositions of these four coatings. Surprisingly, the remaining spectrum (coating 3) shows that for this coating its 1 μm thick upper layer is enriched with silica or/and MEMO-oligomers, as can be concluded from more intense double peak for Si–O–Si stretching at 1090 and 1020 cm^{-1}.

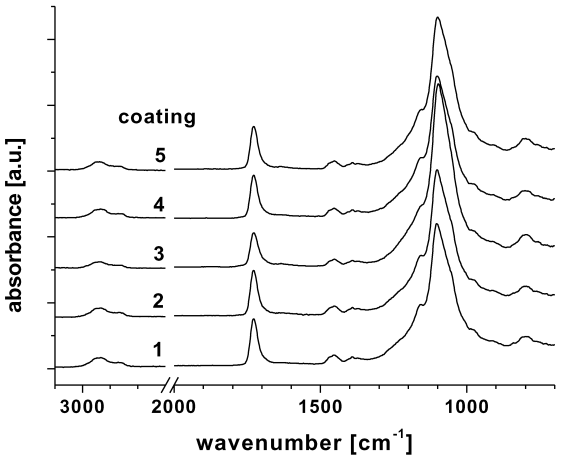

Fig. 13. ATR-IR spectra of the silica–IBMA/HDDA hybrid coatings with the identical chemical composition but the different coating thickness; the coatings 1, 2, 3, 4 and 5, respectively.

The ATR-IR spectra for the first series depending on silica content in IBMA/HDDA organic matrix (coatings 6, 1 and 7 with 10, 20 and 30 vol% of silica, respectively) are shown in Fig. 14. The spectra show that indeed in the upper layers of the coatings the silica content is increased, as can be seen from a comparison of the ratios between silica peaks and, e.g. the C=O stretching vibration or the (anti)symmetric CH_3 and CH_2 stretching vibration.

Approximately the same behavior was found for the silica content series with simultaneous variations in organic matrices, as shown for the coatings 8 and 12 in Fig. 15 and for the coatings 9 and 13 in Fig. 16, respectively.

The absence of an obvious peak corresponding to C=C stretching in four spectra of coating 1 (Fig. 12) suggests that UV curing of the (meth)acrylate matrix was successful throughout the coating thickness. In the other coatings a slightly more pronounced peak for C=C stretching can be observed. This shows that some C=C bonds are left in the coatings 8–15, indicating a lesser UV curing efficiency in

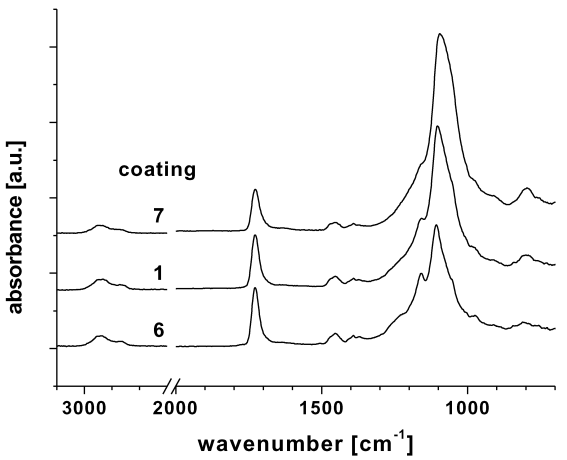

Fig. 14. ATR-IR spectra of the 70 μm thick silica–IBMA/HDDA hybrid coatings with different silica content 10, 20 and 30 vol% in the coatings 6, 1 and 7, respectively.

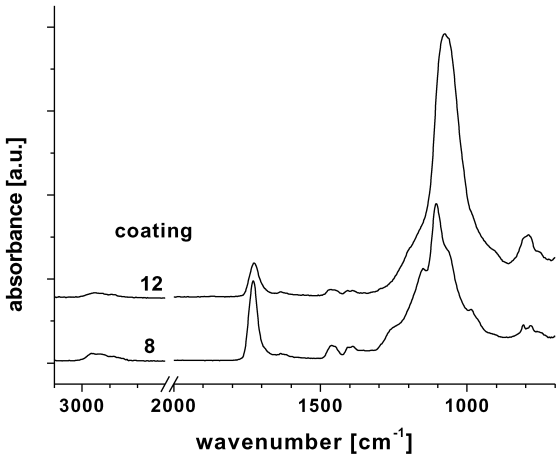

Fig. 15. ATR-IR spectra of the silica–TMPTA hybrid coatings with different silica content 10 and 40 vol% in the coatings 8 and 12, respectively.

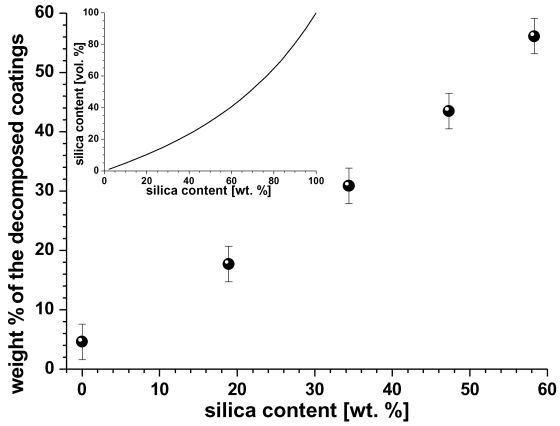

Fig. 17. Wt% of the decomposed coatings versus prescribed wt% of silica. The inclusion provides the vol%/wt% ratio of silica in a silica–(meth)acrylate hybrid system with the materials densities of 2.2 and 1.0 g/cm^3 for silica and (meth)acrylate, respectively.

this series. It also means lower XLD than can be calculated based on the initial amounts added.

Moreover, a thorough examination of the spectra reveals the remarkable tendency that the relative amount of the remaining C=C bonds increases in the top layers of the coatings 8–15 when the silica content is increased from 10 to 40 vol%. Most clearly such a tendency can be seen in the case of the silica–TMPTA/HDDA hybrid coatings (Fig. 16), however, it is also valid for the others: note that despite an increase in silica content by 30 vol%, no noticeable decrease in C=C stretching can be observed (Fig. 15).

It is worth mentioning that for all coatings, besides the coatings made from HEMA (Fig. 1), no noticeable presence of an O–H stretching bond was revealed. This shows that the water content in the coating is minimal.

TGA was used for checking the silica content in each of the coatings. An examination of the TGA graphs for the coatings revealed that the formed MEMO-oligomers were decomposed at a temperature range of 550–800 °C, where a loss in wt% equal to the calculated wt% of the MEMO-oligomers was observed. After grafting the silica particles gained about 3 wt%. This increase in weight was neglected because it was less than the fault of the TGA measurements. The TGA analysis proved that all coatings had the prescribed amount of silica. The weight percentage of the decomposed coatings versus prescribed wt% of silica is shown in Fig. 17 for a decomposition temperature of 900 °C. Remarkably, TGA did not reveal any noticeable deviation of silica content in coating 3 from its prescribed value.

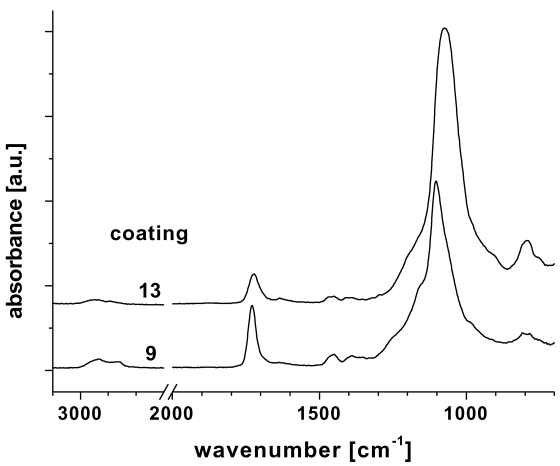

Fig. 16. ATR-IR spectra of the silica–TMPTA/HDDA hybrid coatings with different silica content 10 and 40 vol% in the coatings 9 and 13, respectively.

Additionally, TEM was used to provide the morphological information on a nanometer scale for the silica–(meth)acrylate hybrid coatings. The obtained TEM images for the coatings 11 and 15 are shown in Fig. 18(a) and (b), respectively. The TEM images show that in the HEMA/HDDA matrix the silica particles are present as separated particles homogeneously distributed in coating 11 (10 vol% of silica). In coating 15 (40 vol% of silica) the silica particles are (partly) aggregated into particle network fragments with one particle chain thickness.

3.5. Final thoughts

A comparison of the indentation data and morphological analyses shows that the mechanical properties of the silica–(meth)acrylate hybrid coatings cannot be simply described by the percentage concentration of silica in them, but more insight into the mesoscopic and molecular morphologies of the hybrid systems has to be developed.

In particular, for one of the coatings (coating 3) within the thickness series a higher content of silica or/and MEMO-oligomers in its 1 μm thick upper layer was revealed (Fig. 13), although for the same coating no unusual behavior in the corresponding mechanical measurements was found (Fig. 9). A possible explanation for this obvious

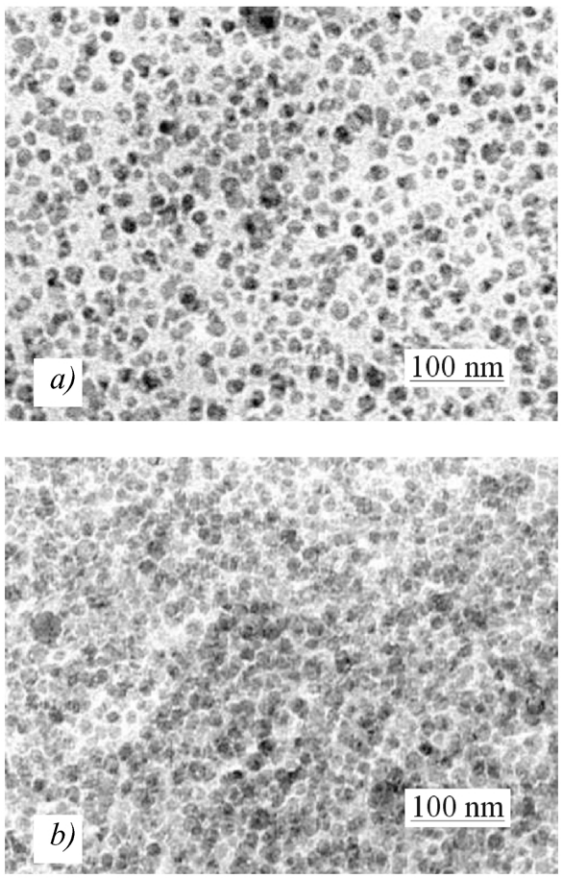

Fig. 18. TEM images for the coatings 11 (a) and 15 (b), respectively.

contradiction may be an inhomogeneous dispersion of MEMO-oligomers through the thickness with a more significant presence of it at the upper layer of the coating. Another reason may be an increase of SiO_2 particle content in the top layer of coating 3 (see below).

When a comparison is made for the IBMA/HDDA coatings with different filler content (FC), the corresponding morphological (Fig. 14) and mechanical (Figs. 10 and 11) data show the expected correlation: an increase in filler particle concentration results in an increase in E_{eff} and H, as has been shown earlier in the literature for silica-filled thermoplastic hybrid coatings for E [38], and in the case of thermoset filled solvent borne coatings for the storage modulus E' [45].

A comparison made of the morphology with aid of ATR-IR and the mechanical properties for the HEMA and TMPTA concentrations series reveals a remarkable contradiction. An increase in silica content from 10 to 40 vol% in the case of the silica–TMPTA hybrid coatings (Fig. 15) is not corresponding to a noticeable increase in E_{eff} and H, as it is normally the case for the rest of the coatings (Table 2). Such a phenomenon was earlier reported for E' by Hill for polyester powder coatings by means of comparing the position of their rubbery plateau [45]. Moreover, van der Linde et al. [46] reported even some reductions in rubbery plateau values of E' for TiO_2 filled coatings comparing to the unfilled ones. Finally, Drozdov and Dorfmann [47] showed that for a carbon black filled elastomer the elastic modulus increases with large particles of filler and decreases with small particles above the percolation threshold. Thus, the final mechanical properties are also dependent on filler size (FS).

Material scientists generally agree that E, $H = f(\mathrm{XLD})$ and, as was reported earlier with increasing XLD, hardness increases [48–50]. The same phenomenon is normally the case for E' as, for instance, was shown for polyallyl diglycol carbonate and polyurethane interpenetrating polymer networks (IPNs) [51] and in the work of Banik and Bhowmick [52]. On the contrary, Mathew et al. [50] showed for IPNs based on natural rubber/polystyrene system that $E = f(\mathrm{XLD})$ is a curve with a maximum in it. In our case HDDA is used as a XLD reducer for the silica–TMPTA/HDDA hybrid coatings due to its lower functionality comparing to TMPTA. Remarkably, that depending on silica content, the influence of XLD is opposite, as for the coatings containing 10 vol% of silica with increasing XLD, E_{eff} and H increase (coatings 8 and 9 in Table 2), and for the coatings containing 40 vol% of silica with increasing XLD, E_{eff} and H decrease (coatings 12 and 13).

Now returning back to the coatings 8 and 12 (Fig. 15 and Table 2), it becomes quite obvious that if an increase in FC or XLD separately results into an increase in E and H, then the only way for E_{eff} of these two coatings to remain approximately constant is that FC and XLD do not influence the mechanical properties of the hybrid coatings independently, but that they influence each other and combined they are responsible for the final mechanical properties. Since modified silica particles also have C=C bonds on their surface, this means that filler content is also responsible for changes in amount and/or type of cross-link density. Thus, it seems to be logical to conclude that an increase of FC decreases cross-link density (or changes its type of cross-links), and this is probably what happens in the case of coatings 12 and 13 too.

A similar explanation can be valid for the untypical IR profile of coating 3 within the thickness series. It means that if the concentration of silica particles in the 1 μm thick upper layer was higher than in the rest of coating 3, it changed the cross-linking in the layer and finally led to unnoticeable changes in the mechanical properties of coating 3 as compared to the rest of the coatings within the thickness series.

Unfortunately, from the series it cannot be estimated how large the influence of increasing of silica content on changing the cross-linking is and this is going to be a topic for our further research.

Furthermore, it is known from the literature that E, $H = f(T_g)$. An increase of E' [53] and H [54] values was reported when the T_g increased, although, it is also claimed that an increase in T_g results in a decrease in XLD [55].

Unfortunately, the T_g of the silica–(meth)acrylate hybrid coatings, reported here, could not be measured and thus no further information is available at this moment.

Thus, after gathering all knowledge together, we end up with a very complex system, in which almost every parameter in some way can be influenced by the others, or saying it differently for the discussed mechanical properties of silica–(meth)acrylate hybrid coatings: E, $H = f(\mathrm{FC}, \mathrm{XLD}, T_g, \mathrm{FS}, \mathrm{CC}, \ldots)$, where cross-link density XLD may be a function of filler content FC and T_g, even when filler size FS is constant.

4. Conclusions

Load and depth sensing indentation has shown itself as a powerful tool for an accurate estimation of mechanical properties of cross-linked and hybrid coatings, as shown for the case of the silica–(meth)acrylate hybrid coatings on polycarbonate substrate. For indentation rates in the range above 2 nm/s the elastic modulus and the hardness appeared to be independent of indentation rate.

The mechanical properties of the silica–(meth)acrylate hybrid coatings, and therefore presumably also of other hybrid systems, cannot be simply predicted and explained by the filler content.

Ideas about mutual influence of cross-link density, filler content and other variables on the mechanical properties of the silica–(meth)acrylate hybrid coatings and simultaneous influence of filler content on cross-link density are given. It is expected that it may be valid for other hybrid polymer systems too.

Acknowledgements

The authors would like to thank Dr J. Malzbender (SVM Laboratory, TU/e, The Netherlands) for useful discussions concerning load and depth sensing indentation measurements and Mr O. van Asselen (SKT Laboratory, TU/e, The Netherlands) for his valuable help in performing and interpreting IR measurements.

References

[1] Tsuchiya S. UK Patent Application No. 8611144; 7 May 1986.
[2] Glotfelter CA, Ryan RP. European Patent Application No. 91301695.2; 1 March 1991.
[3] Revis A, Evans CW. US Patent No. 5.075.348; 24 December 1991.
[4] Kasemann R, Schmidt H. New J Chem 1994;18:1117–23.
[5] Blizzard JD, Cottington LJ. US Patent No. 5.403.535; 4 April 1995.
[6] Medford GF, Patel G. US Patent No. 5.708.048; 13 January 1998.
[7] Medford GF, Gillette GR, Sato N. US Patent No. 5.827.923; 27 October 1998.
[8] Wu S, Sears MT, Soucek MD. Prog Org Coat 1999;36:89–101.
[9] Chen J-I, Chareonsak R, Puengpipat V, Marturunkakul S. J Appl Polym Sci 1999;74:1341–6.
[10] Malzbender J, de With G. J Non-Cryst Solids 2000;265:51–60.
[11] Benitez F, Martinez E, Galan M, Serrat J, Esteve J. Surf Coat Technol 2000;125:383–7.
[12] Malzbender J, de With G, den Toonder JMJ. Thin Solid Films 2000; 372:134–43.
[13] Malzbender J, de With G, den Toonder JMJ. Thin Solid Films 2000; 366:139–49.
[14] Wen J, Wilkes GL. Chem Mater 1996;8:1667–81.
[15] Judeinstein P, Sanchez C. J Mater Chem 1996;6:511–25.
[16] Templin M, Wiesner U, Spiess HW. Adv Mater 1997;9:814–7.
[17] Gilberts J, Tinnemans AHA. RADnews 1998;24:7–10.
[18] Ellsworth MW, Gin DL. Polym News 1999;24:331–41.
[19] Reynaud E, Gauthier C, Perez J. La Ravue de Métallurgie-CTI/ Science et Génie des Matériaux; Février 1999. p. 169–76.
[20] Vales Silva MF, Hancock P, Nicholls JR. Adv Engng Mater 2000;2: 671–5.
[21] Liu E, Shi X, Tan HS, Cheah LK, Sun Z, Tay BK, Shi JR. Surf Coat Technol 1999;120/121:601–6.
[22] Oliver WC, Pharr GM. J Mater Res 1992;7:1564–83.
[23] Doerner MF, Nix WD. J Mater Res 1986;1:601–9.
[24] Wang J, Shi FG, Nieh TG, Zhao B, Brongo MR, Qu S, Rosenmayer T. Scripta Mater 2000;42:687–94.
[25] Friedrich C, Berg G, Broszeit E, Berger C. Thin Solid Films 1996; 290/291:216–20.
[26] Hainsworth SV, Chandler HW, Page TF. J Mater Res 1996;11: 1987–95.
[27] Nix WD. Mater Sci Engng A 1997;234–236:37–44.
[28] Lewis AL, Cumming ZL, Goreish HH, Kirkwood LC, Tolhurst LA, Stratford PW. Biomaterials 2001;22:99–111.
[29] Du B, Liu J, Zhang Q, He T. Polymer 2001;42:5901–7.
[30] Lee EH, Lee Y, Oliver WC, Mansur LK. J Mater Res 1993;8:377–87.
[31] Malzbender J, de With G. Surf Coat Technol 2000;135:60–8.
[32] Loubet JL, Georges JM, Marchesini O, Meille G. J Tribol 1984;106: 43.
[33] Posthumus W, Brokken-Zijp JCM, van der Linde R. In preparation.
[34] Pharr GM. Mater Sci Engng A 1998;253:151–9.
[35] Simmons G, Wang H. Single crystal elastic constants and calculated aggregate properties: a handbook. Cambridge, MA: MIT Press; 1971.
[36] Menčík J. Mechanics of components with treated or coated surfaces. Dordrecht: Kluwer; 1996.
[37] Bolshakov A, Pharr GM. J Mater Res 1998;13:1049–58.
[38] Malzbender J, de With G. J Mater Res 2002;17:502–11.
[39] Malzbender J, den Toonder JMJ, Balkenende R, de With G. Mater Sci Engng Rep A 2002;36:47–103.
[40] Frings S. Organic–inorganic hybrid coatings based on polyester resins and in situ formed silica. PhD Thesis. Universiteitsdrukkerij TU Eindhoven; 1999.
[41] Porter D. Group interaction modeling of polymer properties. New York: Marcel Dekker; 1995.
[42] Drechsler D, Karbach A, Fuchs H. Appl Phys A 1998;66:S825–9.
[43] Soloukhin VA, Brokken-Zijp JCM, de With G. In preparation.
[44] Lin-Vien D, Colthup NB, Fateley WG, Grasselli JG, editors. The handbook of infrared and Raman characteristic frequencies of organic molecules. London: Taylor & Francis; 1991.
[45] Hill LW. J Coat Technol 1991;64:29–41.
[46] van der Linde R, Scholtens BJR, Belder EG. Thermoviscoelastic and thermoanalytical characterization of some reactive polyester powder coating systems. Proceedings of the Eleventh International Conference in Organic Coatings Science and Technology, Athens, Greece; 1987. p. 147.
[47] Drozdov AD, Dorfmann A. Comput Mater Sci 2001;21:395–417.
[48] Hill LW. Mechanical properties of coatings. Federation of Societies for Coating Technology; 1987.
[49] Schwalm R, Haubling L, Reich W, Beck E, Enenkel P, Menzel K. Prog Org Coat 1997;32:191–6.

[50] Mathew AP, Packirisamy S, Radusch HJ, Thomas S. Eur Polym J 2001;37:1921–34.
[51] Dadbin S, Burford RP, Chaplin RP. Polymer 1996;37:785–92.
[52] Banik I, Bhowmick AK. Radiat Phys Chem 1999;54:135–42.
[53] Grunlan JC, Ma Y, Grunlan MA, Gerberich WW, Francis LF. Polymer 2001;42:6913–21.
[54] Wuertz C, Bismarck A, Springer J, Koniger R. Prog Org Coat 1999; 37:117–29.
[55] Sekkar V, Bhagawan SS, Prabhakaran N, Rama Rao M, Ninan KN. Polymer 2000;41:6773–86.